

Modelling and characterization of a pneumatically actuated peristaltic micropump

T. N. Gerasimenko^{1a}, O. V. Kindeeva^{2b}, V. A. Petrov^b, A. I. Khaustov^b and E. V. Trushkin^{3c}

^aLomonosov Moscow State University, Faculty of Physics, Moscow, Russia

^bMoscow Aviation Institute, Moscow, Russia

^cHemule GmbH, Berlin, Germany

December 3, 2024

¹gerasimenko@physics.msu.ru

²ov.kindeeva@gmail.com

³e.trushkin@hemule.de

Abstract

There is an emerging class of microfluidic bioreactors which possess long-term, closed circuit perfusion under sterile conditions with *in vivo*-like flow parameters. Integrated into microfluidics, peristaltic-like pneumatically actuated displacement micropumps are able to meet these requirements. We present a theoretical and experimental characterization of such pumps. In order to examine volume flow rate, we have developed a mathematical model describing membrane motion under external pressure. The viscoelasticity of the membrane and hydrodynamic resistance of the microfluidic channel have been taken into account. Unlike most similar models, the developed model implies only the physical parameters of the pump and allows the estimation of their impact on the resulting flow. The model has been validated experimentally.

1 Introduction

Various microfluidic systems were designed to recreate an *in vivo* microenvironment for cell cultures with regard to physiological mechanical stimulation [1], [2].

A pump providing the circulation of liquid is the key component of these devices [3]. A pump can be either external or integrated into a microfluidic chip [4], [5], [6]. A pump with a pulsatile flow creates significant variations in volume flow rate, affecting the cells by time-varying pressure and shear stress on the cells' surface [7], [8], [9], [6], [10]. Since the production of a pump is a complex process, it is required already at the design stage to understand how the parameters of a pump will affect the resulting flow. In general, fluid-structure interaction modelling is addressable only by numerical simulation [11], [12]. The lumped element model is traditionally used to simplify modelling when the pump is analyzed separately from the microfluidic system and its characteristics are taken as boundary conditions for a liquid flow simulation within a microchannel [13], [14].

A representation of a pump as an equivalent electric circuit is the most common approach for pump modelling [15], [16], [17], [18]. These methods result in flow parameters close to the experimental ones, however, the transition from the pump's physical parameters to the equivalent capacitance, resistance and inductivity is not clear enough. Thus the effect of pump characteristics on flow properties can only be roughly estimated. Moreover, specialized software is required when the equivalent scheme is too complex and branched [15], [19], [16].

The studied pump was a peristaltic-like displacement micropump consisting of two active valves with a working chamber in between. The valves and the working chamber were elastic, pneumatic-actuated membranes organized in a row along a microfluidic channel. Each valve membrane had a strap blocking the channel when the applied pressure was greater than atmospheric pressure (Fig. 1). The valves and the chamber were operated by the proprietary Hemule control unit making the pressure over the membranes either higher (closed valve) or lower (opened valve) than atmospheric pressure. The 6-step algorithm presented in Fig. 2 was implemented in the control unit. All pressure values relate to atmospheric pressure. Frequency is a reciprocal value of one step duration. The six steps together correspond to a single working cycle.

Models of a similar pump have been presented by [20] and [21]. However, the proposed models include experimentally determined empirical parameters with unclear physical meaning thus the major factors affecting volume flow rate remained unidentified. Here we present a mathematical model elucidating how the membranes, microfluidic channel and control unit properties affect the characteristics of the pump.

2 Materials and methods

The micropumps were fabricated in 2 mm polydimethylsiloxane (PDMS) layer using soft lithography [22] and then bonded to a standard 1-mm microscopic glass slide

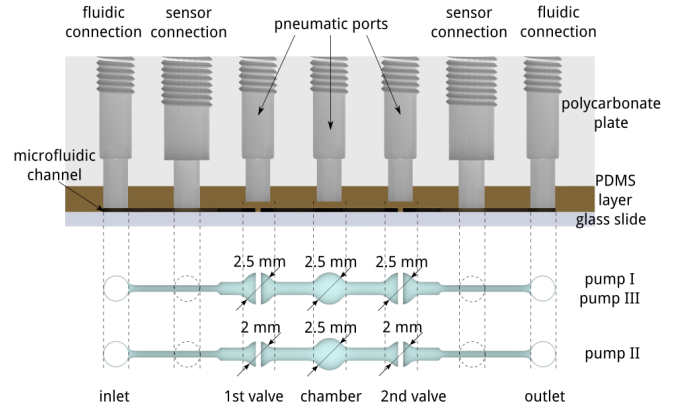


Figure 1: The studied micropumps. All three pumps have a chamber diameter of 2.5 mm and a valve membrane thickness of $530 \pm 5 \mu\text{m}$. Pump I and pump III have valve diameters of 2.5 mm. Pump II has valves with diameters of 2 mm. Pump I and pump II have chamber membrane thicknesses of $530 \pm 5 \mu\text{m}$. Pump III has a chamber membrane with a thickness of $440 \pm 5 \mu\text{m}$.

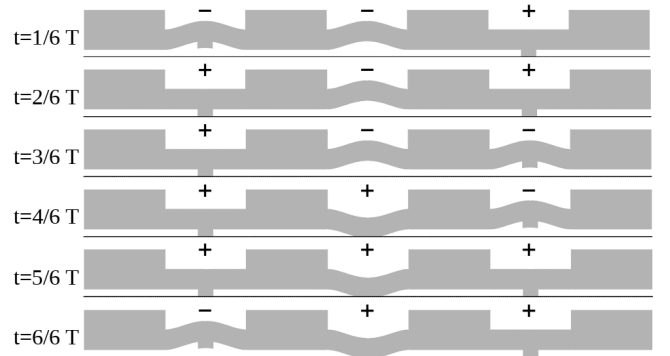


Figure 2: The 6-step algorithm

by means of plasma treatment [23]. The other side of the PDMS layer was based on 10 mm polycarbonate plate with ports for fluidic and pneumatic connections as well as for pressure sensors (Fig. 1). Three versions of the pump were produced to analyze the impact of the pump geometry on its volume flow rate. Two of them (pump I and pump III) had valve diameters of 2.5 mm. Pump II had smaller valves with diameters of 2 mm. All three pumps had a chamber diameter of 2.5 mm (Fig. 3). The thickness h of the membranes was $530 \pm 5 \mu\text{m}$ except for the chamber membrane of pump III ($440 \pm 5 \mu\text{m}$). The pneumatic chamber diameters over the membranes were 2 mm and the channel height was $100 \mu\text{m}$ for all pumps.

PDMS viscoelastic properties were described according to the Kelvin-Voigt model, assuming the following stress-strain relation

$$\sigma(t) = E\varepsilon(t) + \eta\dot{\varepsilon}(t) \quad (1)$$

where $\sigma(t)$ is stress, $\varepsilon(t)$ is strain, E is the PDMS Young modulus and η is its viscosity. The Young modulus of the PDMS strongly depends on the method and conditions of the PDMS preparation [24], therefore we have estimated it by a chamber membrane deflection under a static load

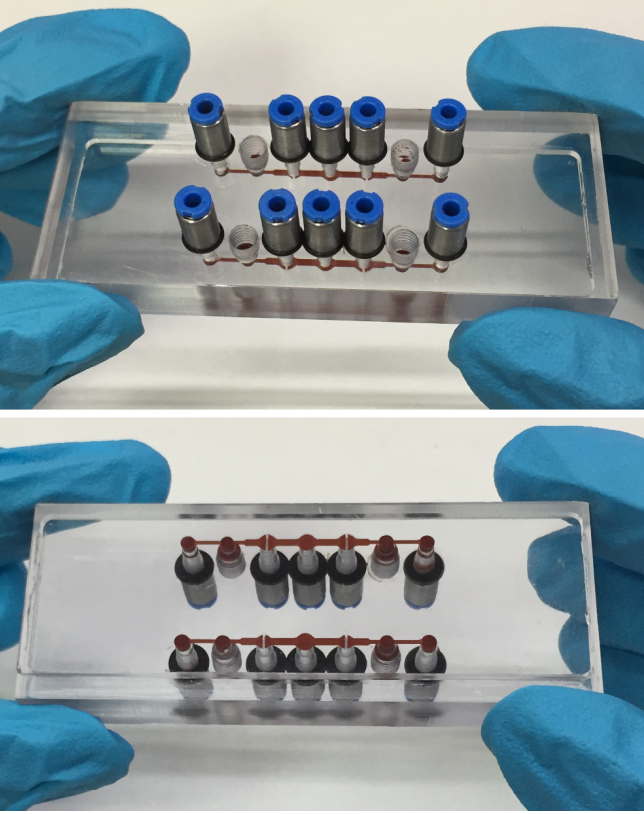


Figure 3: Photo of the device with pumps I and II

as follows [25]:

$$E = \frac{3}{16} \frac{R^4}{h^3} (1 - \nu^2) \frac{p}{w_0}$$

where $\nu = 0.499$ is the Poisson's ratio [24], w_0 is the deflection of the membrane centre from its quiescent position, and p is the pressure over the membrane. In order to measure w_0 , the pump was placed sideways on a stage of the inverted microscope. The static pressure over the working chamber membrane was adjusted using the control unit. The obtained relationship between the membrane centre deflection and the pressure value was approximated by a linear function (Fig. 4).

The obtained Young modulus of 760 ± 140 kPa was in good agreement with the results of [14] and [26].

3 Mathematical model

The developed mathematical model is based on the idea that the volume flow rate caused by each membrane motion can be determined by an integration of membrane velocity over its surface due to the no-slip conditions on a membrane boundary. The velocity has been obtained by solving a membrane motion equation. Since each membrane was actuated by air pressure in pneumatic tubes, first we described the time-dependency of the air pressure.

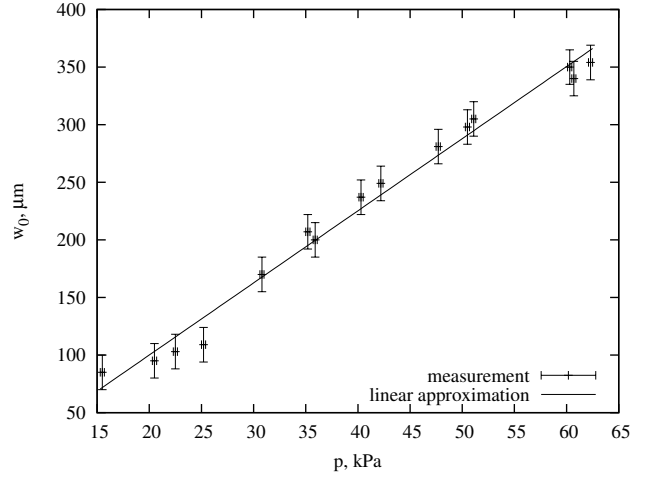


Figure 4: The experimental dependency of the membrane centre deflection on the pressure value

3.1 Time-dependence of the applied pressure

The positive and negative pressures inside the control unit were kept constant, therefore the transient processes of changing pressure were considered as an efflux of air from/to an infinite reservoir according to [27]:

$$\frac{d\eta_{up}}{dt} = A\eta_{up}^{2/7} \sqrt{\eta_{up}^{-2/7} - 1}$$

$$\frac{d\eta_{dn}}{dt} = -A\eta_{dn}^{5/7} \sqrt{1 - \eta_{dn}^{2/7}}$$

for increase and decrease of the pressure correspondingly. $\eta_{up/dn} = p_{up/dn}/p_0$, where p_0 is the pressure provided on the control unit outlets, $p_{up/dn}$ describe the increasing and decreasing pressures correspondingly.

$$A = \frac{R_z \sqrt{T_k} b \tilde{S} \tilde{\mu}}{V}$$

$R_z = 287$ J/kg/K is the specific gas constant for dry air, T_k is air temperature, $b = 0.155$ (kg K/J)^{1/2} and $\tilde{\mu} = 0.8$ are empirical coefficients [27], \tilde{S} is the cross-section of the control unit throttle orifice, V is the total volume of the pneumatic tube and the connection.

The solution of these equations gives the increasing pressure dependency on time in an implicit form:

$$\begin{aligned} (1 - \eta_{up}^{2/7})^{1/2} - \frac{2}{3}(1 - \eta_{up}^{2/7})^{3/2} + \frac{1}{5}(1 - \eta_{up}^{2/7})^{5/2} \\ - (1 - \eta_0^{2/7})^{1/2} + \frac{2}{3}(1 - \eta_0^{2/7})^{3/2} - \frac{1}{5}(1 - \eta_0^{2/7})^{5/2} \\ = -\frac{A}{7}(t - t_0) \end{aligned} \quad (2)$$

and the decreasing one in an explicit form:

$$\eta_{dn} = \left[1 - \left(\sqrt{1 - \eta_0^{2/7}} + \frac{A}{7}(t - t_0) \right)^2 \right]^{7/2} \quad (3)$$

with η_0 being a normalized pressure value at t_0 for each case.

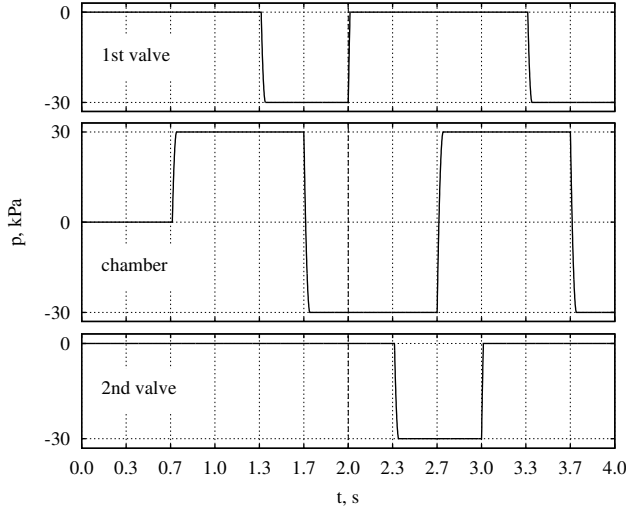


Figure 5: The dependency of the pressure over the valves and chamber membranes on time for $p_0 = 30$ kPa and $\nu = 3$ Hz control unit mode. The dashed line represents the beginning of the 6-step algorithm.

The pneumatic signal edges Δt_{up} and Δt_{dn} were obtained setting $\eta_{up}(t_0 + \Delta t_{up}) = 1$ and $\eta_{dn}(t_0 + \Delta t_{dn}) = 0$ as follows

$$\Delta t_{up} = \frac{7}{A} \left[(1 - \eta_0^{2/7})^{1/2} - \frac{2}{3}(1 - \eta_0^{2/7})^{3/2} + \frac{1}{5}(1 - \eta_0^{2/7})^{5/2} \right]$$

$$\Delta t_{dn} = \frac{7}{A} \left(\sqrt{1 - \eta_0^{2/7}} - 1 \right)$$

Finally the pressure over a membrane was described by the piecewise function of the form:

$$p(t) = \begin{cases} 2p_0(\eta_{up}(t) - 0.5), & t_0 \leq t \leq t_0 + \Delta t_{up} \\ p_0, & t_0 + \Delta t_{up} < t < t_0 + \Delta t_{up} + \delta t \\ 2p_0(\eta_{dn}(t) - 0.5), & t_0 + \Delta t_{up} + \delta t \leq t \leq t_0 + \Delta t_{up} + \delta t + \Delta t_{dn} \\ \dots & \dots \end{cases} \quad (4)$$

where δt is the time span when the pressure remains constant. We neglected possible deformations of valve halves after its strap comes into contact with the channel bottom and assumed that the valve fully stops. Therefore we substituted positive values of pressure bending the valve membrane with zero, since only the membrane bending and not its compression makes a contribution to the flow rate. Fig. 5 represents the corresponding pressures over the valve and chamber membrane for ± 30 kPa and 3 Hz control unit mode. The initial pressure values were assumed to be zero (all membranes are in the quiescent position) for the convenience of following calculations, therefore the 6-step working algorithm begins from 2 s.

3.2 Membrane motion

The membrane was assumed to be isotropic and share deformations were neglected. Since the channel height

was $100 \mu\text{m}$ and the membrane thickness was about $500 \mu\text{m}$, its deflection from the quiescent position was assumed to be low. An application of a general theory for such circular membrane bending [25], [28] to the Kelvin-Voigt stress-strain relationship (1) gives the following initial and boundary value problem for a deflection of the membrane midplane from the quiescent position:

$$\begin{cases} \frac{D}{R^4} \nabla^4 w + \frac{\eta h^3}{12R^4} \nabla^4 \dot{w} + \rho h \ddot{w} = -p(t) - \gamma \dot{w} \\ w(1, t) = 0 \\ w'(1, t) = 0 \\ w(0, t) \rightarrow \infty \\ w(\xi, 0) = 0 \\ \dot{w}(\xi, 0) = 0 \end{cases} \quad (5)$$

where $\dot{w} = \partial w / \partial t$, $w' = \partial w / \partial \xi$, $\xi = r/R$ is the dimensionless radial coordinate, R is the radius of the membrane midplane, ρ is the PDMS density, h is the thickness of the membrane, $\gamma = R_{hyd} \pi R^2$ is the damping coefficient of the channel, R_{hyd} is the hydrodynamic resistance of the channel.

$$D = \frac{Eh^3}{12(1 - \nu^2)}$$

where E is the PDMS Young modulus, ν is Poisson's ratio. The boundary conditions mean the absence of transverse and rotational displacements on the boundary [29]. The membrane displacement is always finite. The initial conditions mean that all membranes were in quiescent position at $t = 0$.

A membrane pushes the liquid through the channel while being deformed. If flow is laminar, the reaction pressure in the channel is proportional to the volume flow rate which depends on the membrane velocity. The damping factor γ represents an averaged factor of proportionality between the channel reaction pressure and velocity of the liquid.

The applied pressure $p(t)$ was calculated according to Section 3.1.

Problem (5) was solved using the eigenfunction expansion technique. Its solution has the following form:

$$w(\xi, t) = \sum_{n=1}^{+\infty} f_n(\xi) g_n(t) \quad (6)$$

where

$$f_n(\xi) = J_0(\lambda_n \xi) - \frac{J_0(\lambda_n)}{I_0(\lambda_n)} I_0(\lambda_n \xi) \quad (7)$$

are the eigenfunctions of the corresponding Sturm-Liouville problem (J_n are Bessel functions of the first kind, I_n are modified Bessel functions of the first kind.) Eigenvalues λ_n were obtained as a solution of the following equation

$$J_0(\lambda_n) I_1(\lambda_n) + I_0(\lambda_n) J_1(\lambda_n) = 0$$

A substitution of expansion (6) into (5) gave the following initial value problem to obtain the functions $g_n(t)$:

$$\begin{cases} \ddot{g}_n + 2\beta_n \dot{g}_n + \omega_{0n}^2 g_n = -\frac{Q_n}{\rho h} p(t) \\ g_n(0) = 0 \\ \dot{g}_n(0) = 0 \end{cases} \quad (8)$$

where

$$\beta_n = \frac{\eta h^2 \lambda_n^4}{24 R^4 \rho} + \frac{\gamma}{2 \rho h} \quad \omega_{0n} = \sqrt{\frac{D}{\rho h}} \left(\frac{\lambda_n}{R} \right)^2$$

$$Q_n = \frac{2}{\lambda_n} \frac{J_1(\lambda_n) - \frac{J_0(\lambda_n)}{I_0(\lambda_n)} I_1(\lambda_n)}{J_1^2(\lambda_n) + \left(\frac{J_0(\lambda_n)}{I_0(\lambda_n)} \right)^2 I_1^2(\lambda_n)}$$

$(Q_n p(t))$ are the expansion coefficients of the pressure $p(t)$ in the eigenfunctions $f_n(\xi)$). Problem (8) represents a well-studied damped harmonic oscillator equation with zero initial conditions. Its solution can be found either numerically or using Green's function:

$$g_n(t) = -\frac{Q_n}{\rho h} \int_0^t e^{-\beta_n(t-\tau)} \frac{\sin[\omega_n(t-\tau)]}{\omega_n} p(\tau) d\tau \quad (9)$$

Thus, the deflection of the membrane midplane from its quiescent position is described by the following dependency

$$w(\xi, t) = -\sum_{n=1}^{+\infty} \frac{Q_n}{\rho h} \left[J_0(\lambda_n \xi) - \frac{J_0(\lambda_n)}{I_0(\lambda_n)} I_0(\lambda_n \xi) \right] \times \int_0^t e^{-\beta_n(t-\tau)} \frac{\sin[\omega_n(t-\tau)]}{\omega_n} p(\tau) d\tau \quad (10)$$

3.3 Volume flow rate

The volume flow is defined as an integration of the obtained membrane velocity over its surface:

$$Q(t) = \int_S \dot{w}(\xi, t) dS \quad (11)$$

To solve this integral curvilinear coordinates were used:

$$x = \xi \cos \varphi \quad y = \xi \sin \varphi \quad z = w(\xi, t)$$

with the following surface area element ([30])

$$dS = \xi \sqrt{1 + (w'(\xi, t))^2} d\xi d\varphi$$

Finally, the volume flow rate has the following form:

$$Q(t) = 2\pi \int_0^1 \dot{w}(\xi, t) \xi \sqrt{1 + (w'(\xi, t))^2} d\xi \quad (12)$$

The chamber membrane is able to reach the channel bottom on the downward motion. The integration lower limit is replaced by $\xi_0(t)$ for this case, being the solution of

$$w(\xi_0, t) = -z_0$$

where z_0 is the height of the channel.

All given calculations have been implemented in C++ using the Boost library to work with Bessel functions.

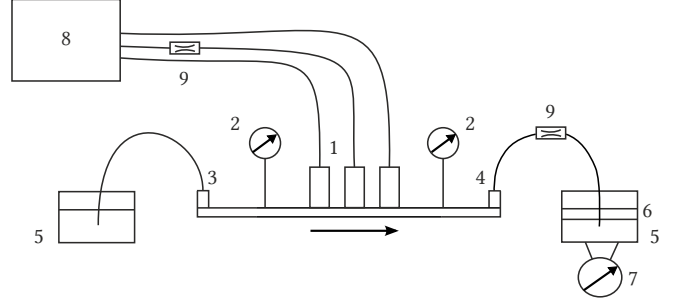


Figure 6: The scheme of the experimental setup: 1 – pump, 2 – pressure sensors, 3 – inlet, 4 – outlet, 5 – water reservoirs, 6 – oil layer, 7 – balance, 8 – control unit, 9 – throttles

4 Experimental setup

The experimental setup is shown schematically in Fig. 6. Each pump was connected to the Hemule control unit “8” using FESTO PUN-H-2×0.4 pneumatic tubes. The same tubes were used to connect inlet “3” and outlet “4” of the pump with reservoirs filled with deionized water “5”. Honeywell 40PC001B pressure sensors “2” were placed as shown in Fig. 1. Their readings were captured by a Tektronix MSO 3024 oscilloscope and converted to pressure units according to the sensor datasheet. The obtained pressure difference $\Delta p(t)$ was converted to the volume flow rate as follows

$$Q(t) = \Delta p(t) \frac{Q_{av}}{\frac{1}{2T} \int_{t_0}^{t_0+T} \Delta p(t) dt}$$

where Q_{av} is the average volume flow rate. In order to measure it, the reservoir connected to the outlet of the pump was placed on an OHAUS EX 224 precision balance “7”. The reservoir was filled with mineral oil “6” to prevent the evaporation of the water from the surface. Division by 2 is caused by the fact that the unclosed pump connection scheme was used in the experiment.

The slope of pressure pulses over the membranes was adjusted by FESTO GRLO-M5-QS-3-LF-C throttles “9” mounted on a pneumatic tubes. The same throttle was used on the outlet tube to simulate the adjustment of friction loss of the microfluidic channel.

5 Results and discussion

Measurements of the volume flow rate were carried out for all versions of the pump. The hydrodynamic resistances were estimated according to [31] and are about 280 Pa·s/mm³ for a channel part between an outlet and a chamber and about 220 Pa·s/mm³ for a part between an outlet and a valve. PDMS viscosity was taken to be 32 kPa·s [32]. Experimental results (Fig. 7) show that valves with a smaller diameter produce peaks with a smaller magnitude (pump I and pump II), whereas the working chamber with a thinner membrane produces a higher peak (pump I and pump III). These results are in close agreement with theoretical predictions (Fig. 8).

Some discrepancy between the theory and the experiment is observed when a valve opens. It happens probably due to the non-laminar transitional flow when the strap of a valve is detached from the bottom of the channel and the fluid flows under it. Consideration of this transition process is beyond the scope of this paper.

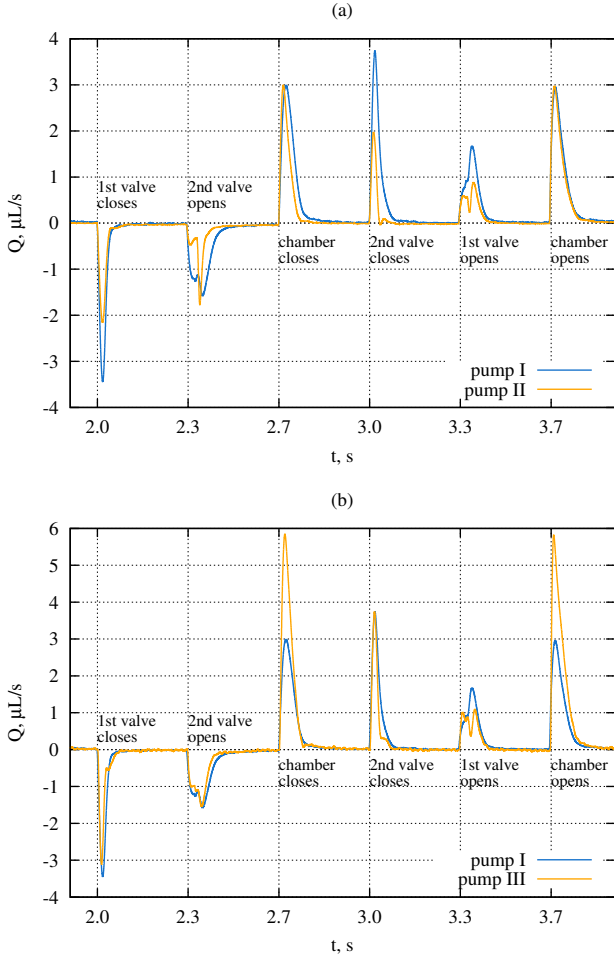


Figure 7: Comparison of volume flow rates generated by (a) pump I and pump II (smaller valves) and (b) pump I and pump III (thinner working chamber membrane)

Average volume flow rates over one pumping cycle for all types of the pump and for different control unit modes are represented in Fig. 9. As follows from these results, the average volume flow rate is proportional to the pumping frequency and the pressure magnitude until the chamber membrane reaches the channel bottom. The theoretically predicted average volume flow rates are equal for pump I and pump II because the contributions of valves compensate for each other if the valve properties are identical. The measured data coincides within a measurement error.

Fig. 10 represents theoretical dependencies of flow rate peak created by the chamber membrane with different pump parameters. The investigated parameters were the membrane radius (Fig. 10a) and thickness (Fig. 10b), as well as the hydraulic resistance of the channel after the pump (Fig. 10c) and the slope of the air pressure pulse over the membrane (Fig. 10d). The last was governed

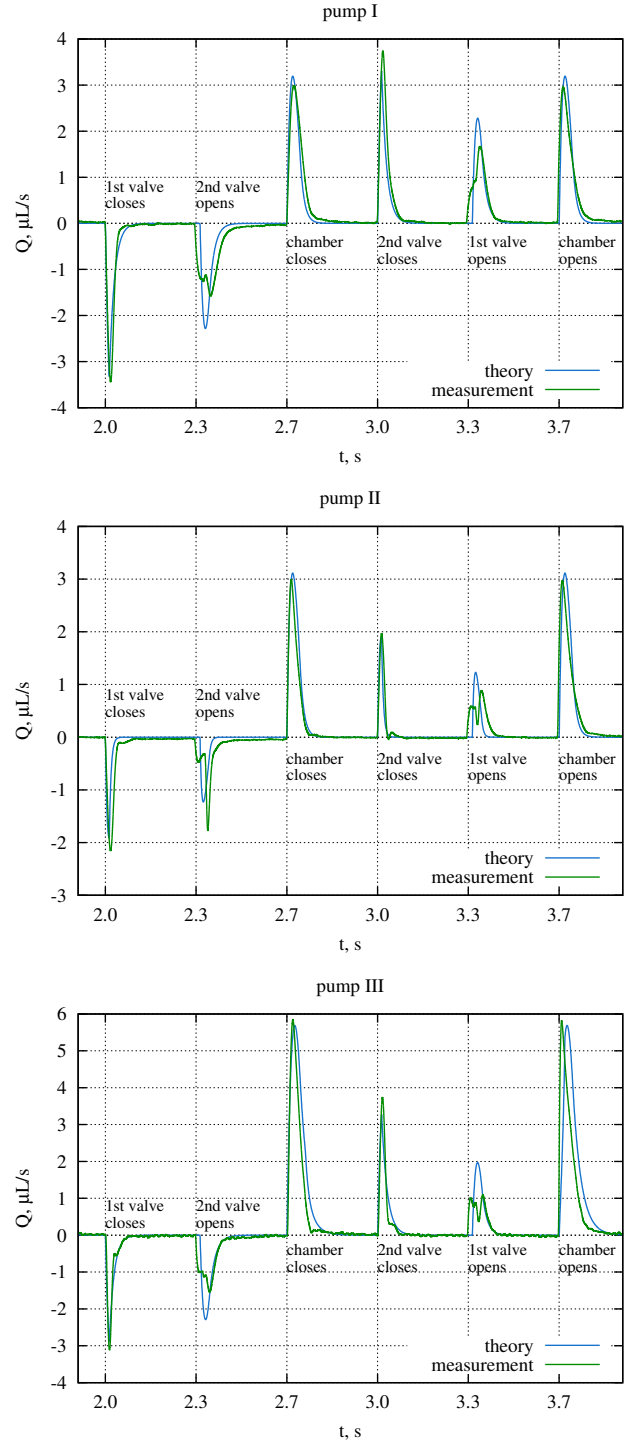


Figure 8: Comparison between the experimental results and the theoretical predictions

by throttles connected to the control unit outputs. (The smaller the throttle orifice, the gentler the slope.)

A curve break corresponds to the membrane reaching the bottom of the channel. The experimental evidence for the influence of the membrane radius and thickness on the peak form can be seen in Fig. 7 and 8. The qualitative experimental dependency of the peak on the hydrodynamic resistance of a channel is shown in Fig. 11. The hydrodynamic resistance was changed by varying the cross-section of the throttle connected to the outlet.

Such throttle does not influence data obtained from a sensor placed closer to the inlet, therefore only the data from the sensor placed closer to the outlet is shown. The obtained curve represents the contribution to the flow rate of a valve nearest to the sensor and a chamber when this valve is open.

Similar measurements were carried out in order to study the dependency of the peak on the pressure slope. The latter is determined by a pneumatic tube orifice (Section 3.1) and was changed with a throttle mounted on a pneumatic tube, that operates the pressure over the membrane of the chamber. The corresponding data from a sensor placed closer to the pump outlet is shown in Fig. 12. All measurements were made using pump III.

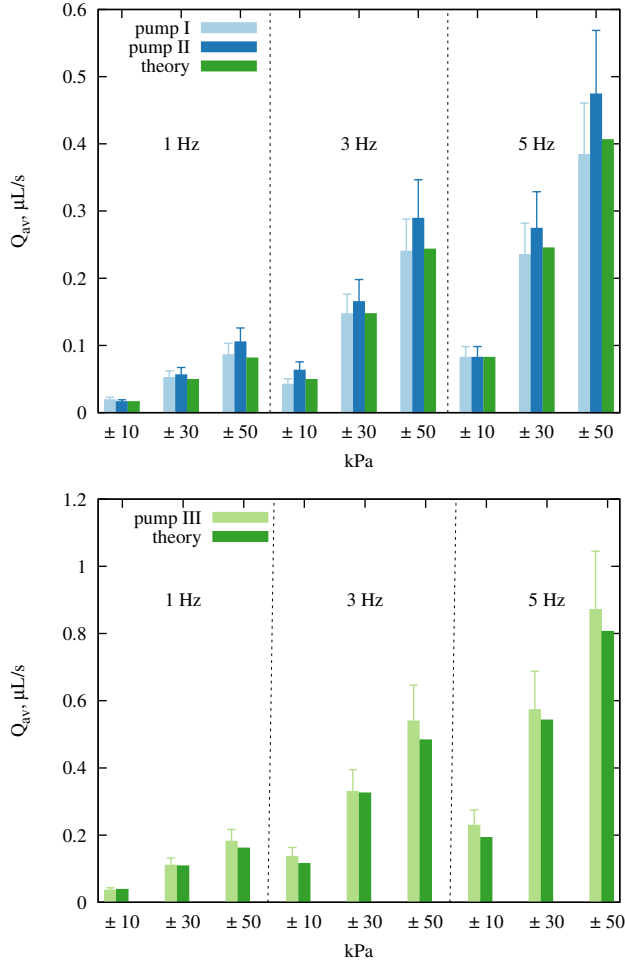


Figure 9: The average volume flow rate of investigated pumps compared with theory

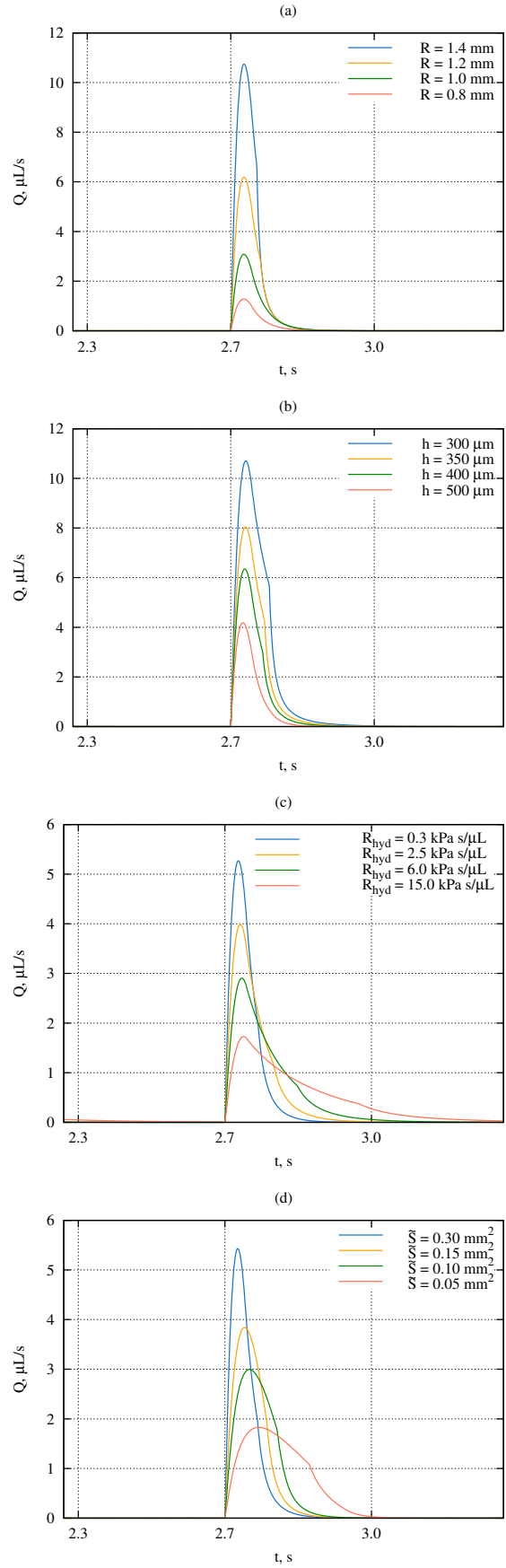


Figure 10: The impact of a membrane radius (a), its thickness (b), hydrodynamic resistance of a channel (c) and the slope of the pressure pulse (determined by \dot{S}) on the form of the peak created by the chamber of pump III

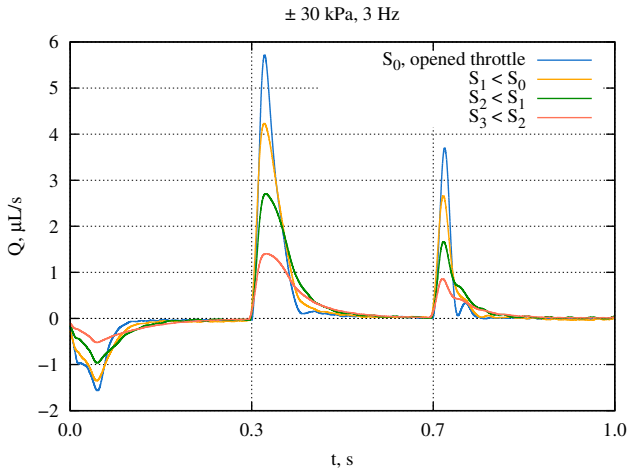


Figure 11: The throttle is mounted on the outlet to increase the hydrodynamic resistance after the pump. The Figure shows peaks obtained from the outlet pressure sensor for different throttle cross-sections.

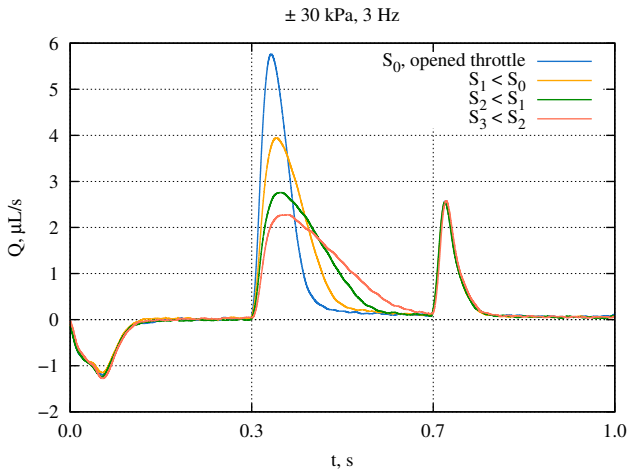


Figure 12: The slope of the pressure pulse is changed by varying the control unit throttle cross-section. The Figure shows peaks obtained from the outlet pressure sensor for different throttle cross-sections.

6 Conclusion

The developed mathematical model provides the volume flow rate created by a peristaltic-like displacement micropump with active valves by a point-blank description of the membrane motion. The material of the membrane (PDMS) was assumed to be isotropic, viscoelastic and was described using the Kelvin-Voigt model. The hydrodynamic resistance of a microfluidic channel was also considered. A number of assumptions were made in order to simplify the solution. Namely, the channel walls were assumed to be stiff, the valves were expected to fully stop when their strap reached the bottom of the channel, and in this case the velocity of the chamber membrane was considered equal to zero. The predictions

of the model are in a good agreement with experimental results. The main advantage of the developed model is the fact that it only uses the physical parameters of the pump and allows the estimation of their influence on the resulting flow. On the other hand it does not require sophisticated software for implementation. The model can be used to describe other pumps working on a similar principle and to obtain boundary conditions when calculating flow in microfluidic channels. Since the calculation performed in Section 3.2 did not use an explicit form of the applied pressure $p(t)$, one can substitute any other force into the right-hand side of the equation and thus use this model to describe pumps with other actuation types.

References

- [1] Dongeun Huh, Benjamin D Matthews, Akiko Mamoto, Martín Montoya-Zavala, Hong Yuan Hsin, and Donald E Ingber. Reconstituting Organ-Level Lung Functions on a Chip. *Science*, 328(5986): 1662–1668, 2010. doi: 10.1126/science.1188302.
- [2] Dongeun Huh, Geraldine A. Hamilton, and Donald E. Ingber. From 3D cell culture to organs-on-chips. *Trends Cell Biol.*, 21(12):745–754, 2011. ISSN 09628924. doi: 10.1016/j.tcb.2011.09.005.
- [3] Min-Hsien Wu, Song-Bin Huang, and Gwo-Bin Lee. Microfluidic cell culture systems for drug research. *Lab Chip*, 10(8):939–956, 2010. ISSN 1473-0197. doi: 10.1039/b921695b.
- [4] D J Laser and J G Santiago. A review of micropumps. *J. Micromechanics Microengineering*, 14(6): R35–R64, 2004. ISSN 0960-1317. doi: 10.1088/0960-1317/14/6/R01.
- [5] Brian D. Iverson and Suresh V. Garimella. Recent advances in microscale pumping technologies: a review and evaluation. *Microfluid. Nanofluidics*, 5(2):145–174, 2008. ISSN 1613-4982. doi: 10.1007/s10404-008-0266-8.
- [6] Song-Bin Huang, Shih-Siou Wang, Chia-Hsun Hsieh, Yung Chang Lin, Chao-Sung Lai, and Min-Hsien Wu. An integrated microfluidic cell culture system for high-throughput perfusion three-dimensional cell culture-based assays: effect of cell culture model on the results of chemosensitivity assays. *Lab Chip*, 13(6):1133–1143, 2013. ISSN 1473-0189. doi: 10.1039/c2lc41264k.
- [7] C.R. Jacobs, C.E. Yellowley, B.R. Davis, Z. Zhou, J.M. Cimbala, and H.J. Donahue. Differential effect of steady versus oscillating flow on bone cells. *J. Biochem*, 31(11):969–976, 1998. ISSN 15378276. doi: 10.1016/j.biotechadv.2011.08.021.Secreted.
- [8] Tzung K. Hsiai, Sung K. Cho, Henry M. Honda, Susan Hama, Mohamad Navab, Linda L. Demer, and Chih Ming Ho. Endothelial cell dynamics under pulsating flows: Significance of high versus low shear

- stress slew rates. *Ann. Biomed. Eng.*, 30(5):646–656, 2002. ISSN 00906964. doi: 10.1114/1.1484222.
- [9] M T van der Pauw, J Klein-Nulend, T van den Bos, E H Burger, V Everts, and W Beertsen. Response of periodontal ligament fibroblasts and gingival fibroblasts to pulsating fluid flow: nitric oxide and prostaglandin E2 release and expression of tissue non-specific alkaline phosphatase activity. *J Periodontal Res*, 35(6):335–343, 2000. ISSN 0022-3484. doi: 10.1034/j.1600-0765.2000.035006335.x.
- [10] Wan-Ying Lin, Yu-Han Chang, Hsin-Yao Wang, Tzu-Chi Yang, Tzu-Keng Chiu, Song-Bin Huang, and Min-Hsien Wu. The study of the frequency effect of dynamic compressive loading on primary articular chondrocyte functions using a microcell culture system. *BioMed Research Int.*, 2014(1):762570–762582, 2014. ISSN 2314-6141. doi: 10.1155/2014/762570.
- [11] Chakraborty Debad, Prakash J. Ravi, Leslie Yeo, and James Friend. Fluid-Structure Interaction in Deformable Microchannels. *Phys. Fluids*, 24:102002–102037, 2012. doi: 10.1063/1.4759493.
- [12] Osman Omran Osman, Atsushi Shirai, and Satoyuki Kawano. A numerical study on the performance of micro-vibrating flow pumps using the immersed boundary method. *Microfluid. Nanofluidics*, 19(3):595–608, 2015. ISSN 1613-4982. doi: 10.1007/s10404-015-1586-0.
- [13] F Goldschmidtböing, A Doll, M Heinrichs, P Woias, H-J Schrag, and U T Hopt. A generic analytical model for micro-diaphragm pumps with active valves. *J. Micromechanics Microengineering*, 15(4):673–683, 2005. ISSN 0960-1317. doi: 10.1088/0960-1317/15/4/001.
- [14] Chengpeng Yang, Dinglong Hu, Baoce Sun, Xin Cui, Qian Zhu, and Raymond H. W. Lam. Mixing in an enclosed microfluidic chamber through moving boundary motions. *Microfluid. Nanofluidics*, 19(3):711–720, 2015. ISSN 1613-4982. doi: 10.1007/s10404-015-1596-y.
- [15] Tarik Bourouina and Jean-Paul Grandchamp. Modeling micropumps with electrical equivalent networks. *J. Micromechanics Microengineering*, 6(4):398–404, 1996. ISSN 0960-1317. doi: 10.1088/0960-1317/6/4/006.
- [16] Elisa Morganti, Iolanda Fuduli, Andrea Montefusco, Marco Petasecca, and U. Giorgio Pignatelli. SPICE modelling and design optimization of micropumps. *Int. J. Environ. Anal. Chem.*, 85(9-11):687–698, 2005. ISSN 0306-7319. doi: 10.1080/03067310500153876.
- [17] Jacques Goulpeau, Daniel Trouchet, Armand Ajdari, and Patrick Tabeling. Experimental study and modeling of polydimethylsiloxane peristaltic micropumps. *J. Appl. Phys.*, 98(4):1–9, 2005. ISSN 00218979. doi: 10.1063/1.1947893.
- [18] Chun-Wei Huang, Song-Bin Huang, and Gwo-Bin Lee. Pneumatic micropumps with serially connected actuation chambers. *J. Micromechanics Microengineering*, 16(11):2265–2272, 2006. ISSN 0960-1317. doi: 10.1088/0960-1317/16/11/003.
- [19] Samir Bendib and Olivier Francais. Analytical study of microchannel and passive microvalve : “Application to Micropump simulator”. In *Des. Charact. Packag. Mem Microelectron. Ii*, volume 4593, pages 283–291, 2001. ISBN 0-8194-4323-9. doi: 10.1117/12.448859.
- [20] Oana Tatiana Nedelcu, Jean-Luc Morelle, Catalin Tibeica, Samuel Voccia, Irina Codreanu, and Severin Dahms. Modelling and simulation of a pneumatically actuated micropump. In *Semicond. Conf. 2007. CAS 2007. Int.*, volume 1, pages 77 – 80, 2007. ISBN 978-1-4244-0847-4.
- [21] M. Busek, M. Nötzel, C. Polk, and F. Sonntag. Characterization and simulation of peristaltic micropumps. *J. Sensors Sens. Syst.*, 2(2):165–169, 2013. ISSN 2194-878X. doi: 10.5194/jsss-2-165-2013.
- [22] Marc A Unger, Hou-Pu Chou, Todd Thorsen, Axel Scherer, and Stephen R Quake. Monolithic Microfabricated Valves and Pumps by Multilayer Soft Lithography. *Science*, 288:113–116, 2000.
- [23] Michael J. Owen and Jennifer L. Stasser. Plasma treatment of polydimethylsiloxane. *J. Adhes. Sci. Technol.*, 8(10):1063–1075, 1994. ISSN 00323934. doi: 10.1163/156856194X00942.
- [24] I D Johnston, D K McCluskey, C K L Tan, and M C Tracey. Mechanical characterization of bulk Sylgard 184 for microfluidics and microengineering. *J. Micromechanics Microengineering*, 24(3):035017 – 035024, 2014. ISSN 0960-1317. doi: 10.1088/0960-1317/24/3/035017.
- [25] J. N. Reddy. *Theory and Analysis of Elastic Plates and Shells*. CRC Press, 2nd edition, 2006.
- [26] D. Armani, C. Liu, and N. Aluru. Re-configurable fluid circuits by PDMS elastomer micromachining. In *Twelfth IEEE Int. Conf. Micro Electro Mech. Syst.*, pages 222–227, 1999. ISBN 0-7803-5194-0. doi: 10.1109/MEMSYS.1999.746817.
- [27] M Z Kolovsky. *Nonlinear Dynamics of Active and Passive Systems of Vibration Protection*. Springer-Verlag Berlin Heidelberg, 1999. ISBN 9783662222362.
- [28] S B Singh and M Arif. Vibration analysis of viscoelastic clamped circular plates subjected to thermal gradient. *Indian J. Eng. Matherial Sci.*, 9(5):103–108, 2002.
- [29] Ranesh Sircar. Dynamic response of circular plates on elastic foundation subjected to sonic booms. *Indian J. Pure Appl. Math.*, 6(5):530–538, 1973.

- [30] G M Fichtenholz. *The fundamentals of mathematical analysis*. Oxford : Pergamon, 1965.
- [31] Henrik Bruus. *Theoretical Microfluidics*. Oxford University Press, 2008. ISBN 978-0-19-923508-7.
- [32] Frank E. Swallow. Viscosity of polydimethylsiloxane gum: Shear and temperature dependence from dynamic and capillary rheometry. *J. Appl. Polym. Sci.*, 84(13):2533–2540, 2002. ISSN 00218995. doi: 10.1002/app.10563.